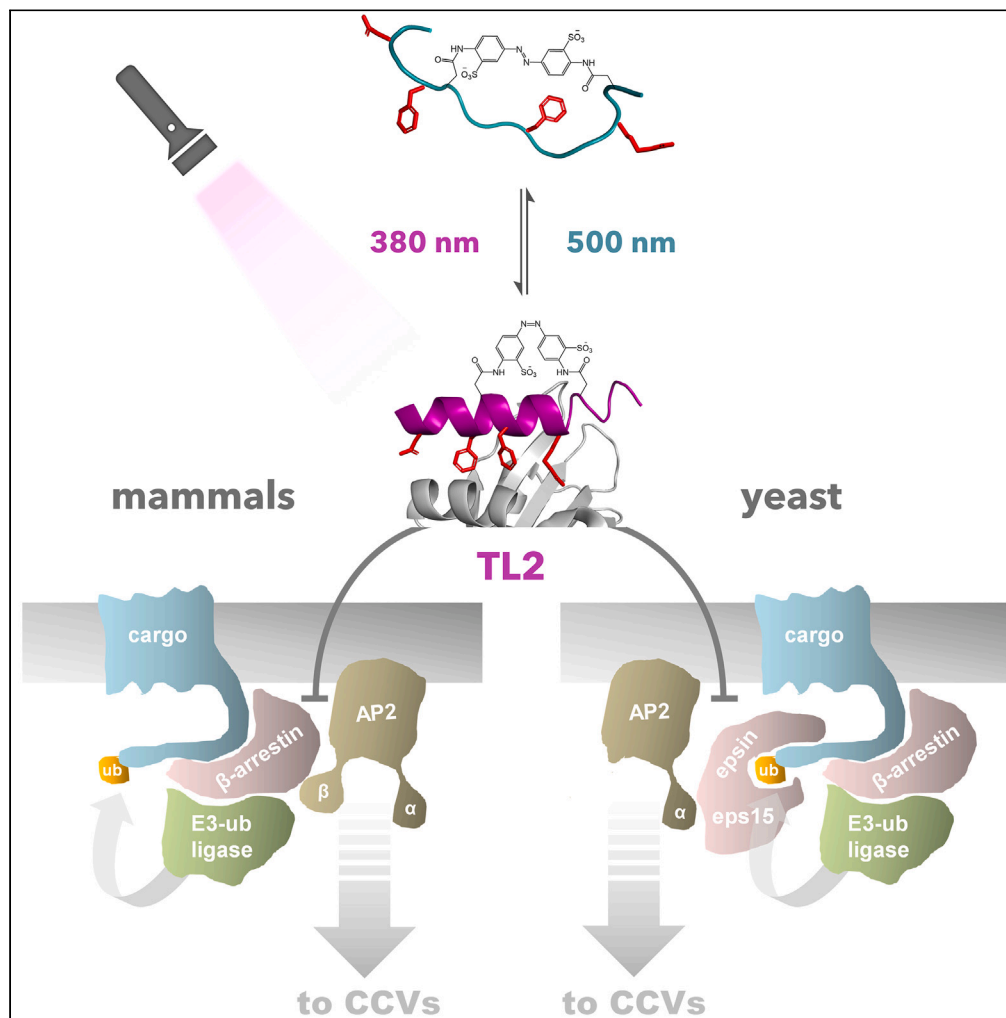**Article**

Light-dependent inhibition of clathrin-mediated endocytosis in yeast unveils conserved functions of the AP2 complex

Davia Prischich,
Núria Camarero,
Javier Encinar del
Dedo, ..., Ernest
Giralt, María Isabel
Geli, Pau Gorostiza

mgfbmc@ibmb.csic.es (M.I.G.)
pau@icrea.cat (P.G.)

Highlights
Traffic Light peptide TL2 is a photoswitchable inhibitor of CME in yeast

TL2 targets yeast α-adaptin, unveiling relevant Eps15 and epsin/AP2 interactions

Acute inhibition of yeast AP2 uncovers previously unnoticed endocytic functions

Conserved molecular interfaces execute similar endocytic functions

Article

Light-dependent inhibition of clathrin-mediated endocytosis in yeast unveils conserved functions of the AP2 complex

Davia Prischich,[1,2,8] Núria Camarero,[1,2] Javier Encinar del Dedo,[3,9] Maria Cambra-Pellejà,[1] Judit Prat,[1] Laura Nevola,[4,10] Andrés Martín-Quirós,[1,11] Elena Rebollo,[5] Laura Pastor,[3] Ernest Giralt,[4,6] María Isabel Geli,[3,*] and Pau Gorostiza[1,2,7,12,*]

SUMMARY

Clathrin-mediated endocytosis (CME) is an essential cellular process, conserved among eukaryotes. Yeast constitutes a powerful genetic model to dissect the complex endocytic machinery, yet there is a lack of specific pharmacological agents to interfere with CME in these organisms. TL2 is a light-regulated peptide inhibitor targeting the AP2-β-adaptin/β-arrestin interaction and that can photocontrol CME with high spatiotemporal precision in mammalian cells. Here, we study endocytic protein dynamics by live-cell imaging of the fluorescently tagged coat-associated protein Sla1-GFP, demonstrating that TL2 retains its inhibitory activity in _S. cerevisiae_ spheroplasts. This is despite the β-adaptin/β-arrestin interaction not being conserved in yeast. Our data indicate that the AP2 α-adaptin is the functional target of activated TL2. We identified as interacting partners for the α-appendage, the Eps15 and epsin homologues Ede1 and Ent1. This demonstrates that endocytic cargo loading and sensing can be executed by conserved molecular interfaces, regardless of the proteins involved.

INTRODUCTION

Clathrin-mediated endocytosis (CME) is one of the major entry routes for extracellular material and plasma membrane (PM) into eukaryotic cells. The process is essential to internalize nutrients, to maintain PM homeostasis, and to regulate receptor turnover and signaling, among other cellular functions. Endocytic vesicles are also employed by pathogenic toxins,[1–3] bacteria,[4] and viruses[5] (including SARS-CoV-2)[6,7] to reach intracellular compartments, whereas dysfunctions in the pathway can result in several diseases including cancer, myopathies, and neuropathies.[8] The formation of an endocytic vesicle relies on the sequential and finely coordinated assembly of more than 60 molecular actors which are conserved between yeast and mammalian cells. Thus, _Saccharomyces cerevisiae_ provides a convenient model system to study the process, delivering findings that can often be extrapolated to higher eukaryotes.[9–11] Yeast amenability to genetic manipulation, together with advances in live-cell fluorescence microscopy and time-resolved electron microscopy, has allowed to examine CME dynamics with great spatiotemporal resolution, and couple the recruitment of particular proteins to specific membrane deformation steps.[12–17]

Several strategies can be used to selectively interfere with CME in order to study the role of specific interactions between endocytic proteins and to decipher the impact of CME on particular cellular processes. Classic genetic manipulation is time-consuming and not straightforward, and it can result in compensatory cellular responses that complicate the interpretation of the results. In addition, loss-of-function mutations may result in non-viable strains or display pleiotropic phenotypes when the proteins involved have multiple functions. Reciprocally, genetic redundancy might hinder uncovering of _bona fide_ protein functions. These limitations have prompted the search for chemical and pharmacological agents that can specifically, acutely, and reversibly manipulate CME.[18] However, only few chemical tools are known to effectively and specifically inhibit CME, and none of them has been reported to be effective in yeast (Figure 1A).[19,20] To date, the actin

[1]Institute for Bioengineering of Catalonia (IBEC), The Barcelona Institute of Science and Technology, Barcelona, Spain
[2]Centro de Investigación Biomédica en Red – Bioingeniería, Biomateriales y Nanomedicina (CIBER-BBN), Barcelona, Spain
[3]Department of Cell Biology, Institute for Molecular Biology of Barcelona (IBMB-CSIC), Barcelona, Spain
[4]Institute for Research in Biomedicine (IRB Barcelona), The Barcelona Institute of Science and Technology, Barcelona, Spain
[5]Molecular Imaging Platform, Institute for Molecular Biology of Barcelona (IBMB-CSIC), Barcelona, Spain
[6]Department of Inorganic and Organic Chemistry, University of Barcelona (UB), Barcelona, Spain
[7]Catalan Institution for Research and Advanced Studies (ICREA), Barcelona, Spain
[8]Present address: Department of Chemistry, Molecular Sciences Research Hub, Imperial College London, London, United Kingdom
[9]Present address: Institute of Functional Biology and Genomics, Salamanca, Spain
[10]Present address: IDP Discovery Pharma, Parc Científic de Barcelona (PCB), Barcelona, Spain
[11]Present address: Ernst & Young, Barcelona, Spain
[12]Lead contact
*Correspondence: mgfbmc@ibmb.csic.es (M.I.G.), pau@icrea.cat (P.G.)
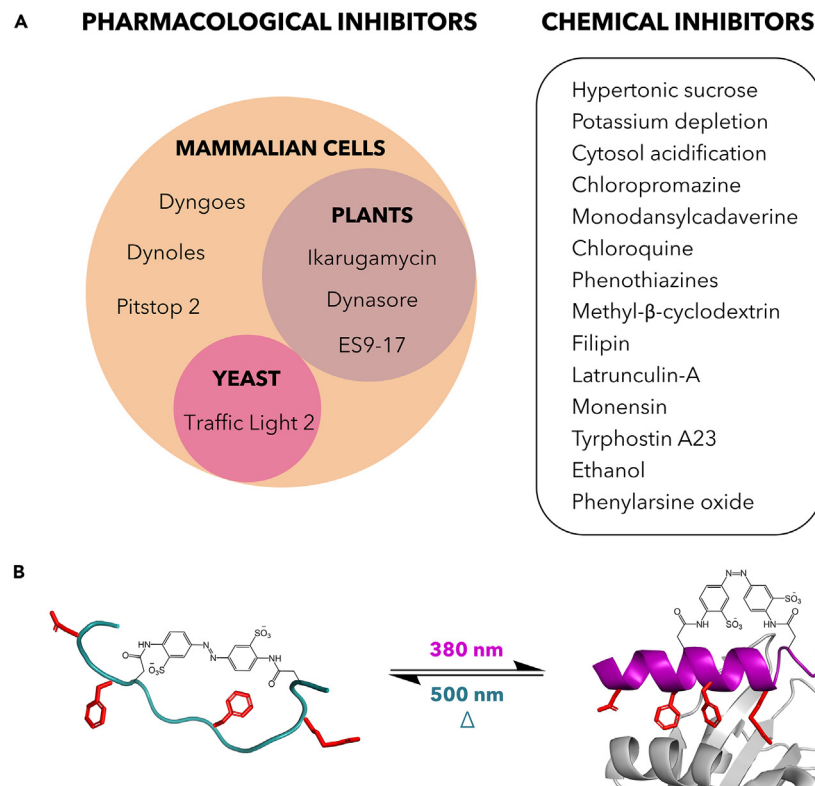https://doi.org/10.1016/j.isci.2023.107899

Figure 1. Clathrin-mediated endocytosis (CME) inhibitors

(A) On the left, pharmacological agents targeting specific endocytic proteins classified according to their biological activity in mammalian cells, plants, and yeast. On the right, chemicals that perturbate CME via a pleiotropic mechanism of action. Limits and advantages of each approach have been covered in the literature.[18,19,22–24]

(B) Traffic Light 2 (TL2) and its structural alterations produced by exposure to light. Upon illumination with UV light (380 nm), the crosslinker photoisomerizes from *trans* (dark-adapted conformation) to *cis*, thus promoting a helical structure (on the right, in purple) and the correct orientation of those residues (in red) responsible for the interaction with AP2 (in gray). Exposure to green light (500 nm) or spontaneous thermal relaxation revert the crosslinker to its stable conformation, thus causing partial unfolding of the peptide and loss of activity (on the left, in green).

polymerization inhibitor Latrunculin A and the sterol sequestering filipin have been used to manipulate endocytic uptake in yeast, but they have pleiotropic effects in many other cellular functions.[20,21]

Thus, it would be very useful to identify a pharmacological agent capable of interfering with CME in a specific, acute, and reversible way in yeast, to take advantage of this well-defined model for the study of endocytosis. Previously, Nevola et al. developed two Traffic Lights (TLs), photoswitchable inhibitors of CME.[25] TLs are based on the structure of the human β-arrestin C-terminal peptide (BAP-long), which binds to the appendage of the β2-adaptin subunit of AP2, the major endocytic clathrin adaptor in mammalian cells.[26,27] Light regulation was introduced by stapling the structures with a photoresponsive bridge that upon *trans-cis* isomerization can modulate the helical content, and therefore, the inhibitory activity of the peptides.[28,29] When tested in mammalian cells, both TLs blocked CME in a light-regulated manner. Between the two, Traffic Light 2 (TL2) proved particularly attractive as it is inert under dark-adapted conditions (*trans* isomer), but it strongly reduces CME trafficking upon activation with (ultra)violet light (*cis* isomer) (Figure 1B). Here, we demonstrate that the TL2 peptide designed for mammalian proteins retains its activity in yeast and provides a powerful tool to dynamically regulate CME. Interestingly, our *in silico* and experimental data indicate that TL2 interferes with α-adaptin binding to Eps15 and epsin homologues. No endocytic defects were previously reported for the constitutive knock-out strains of any of the AP2 subunits in *S. cerevisiae*[30,31] whereas activated TL2 treatment unveiled conserved functions for AP2 in yeast, thus demonstrating its experimental power. The results also raise the interesting possibility that particular endocytic functions, such as cargo recruitment to clathrin-coated pits, might be executed by interactions between analogous molecular surfaces, regardless of the particular proteins involved. In this context, photoswitchable peptides that target those conserved molecular landscapes might be ideal tools to universally interfere with such endocytic functions.

RESULTS

Uptake and intracellular distribution of TL2 peptide in *S. cerevisiae* spheroplasts

Although some peptides have been reported to penetrate the fungal cell wall, this remains a prohibitive barrier to most macromolecules.[32] Since TL2 targets an intracellular protein-protein interaction, we first tested whether it could be internalized in yeast using an analogue
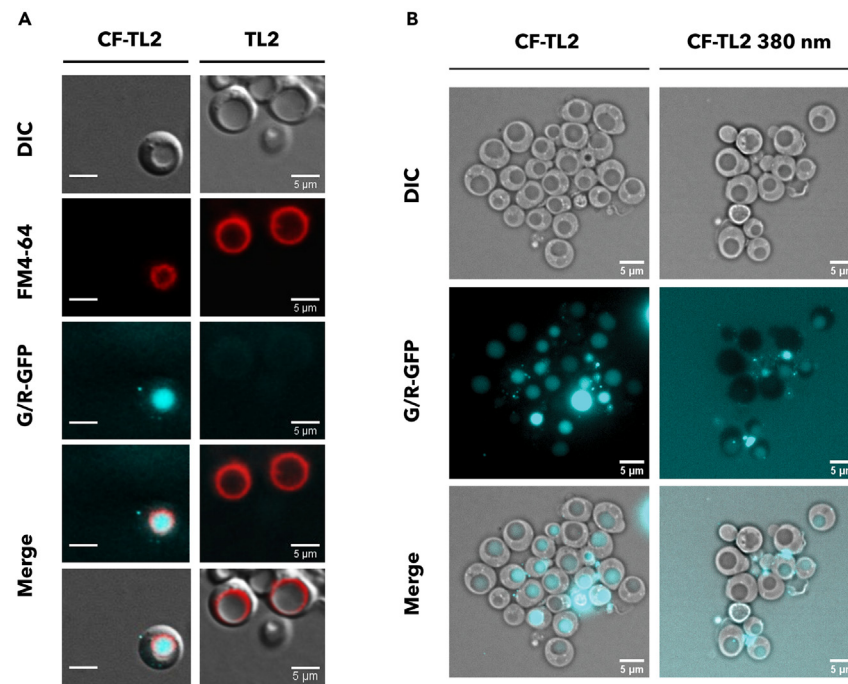
Figure 2. Uptake and intracellular distribution of TL2 in *S. cerevisiae* spheroplasts

(A) Differential Interference Contrast (DIC) (upper panels) and fluorescence micrographs of *S. cerevisiae* cells loaded for 5 min at 25°C with FM4-64 (16 μM), washed and incubated for 40 min with 30 μM of either dark-adapted (inactive) carboxyfluorescein conjugated TL-2 (CF-TL2) or TL2 as control. The individual channels and the merged images of the fluorescein and FM4-64 channels, and the DIC, fluorescein and FM4-64 channels are shown.

(B) DIC (upper panels) and fluorescence micrographs of *S. cerevisiae* cells incubated for 40 min at 25°C with 30 μM of either dark-adapted (inactive) carboxyfluorescein conjugated TL-2 (CF-TL2) or pre-illuminated (active) carboxyfluorescein conjugated TL-2 peptide (CF-TL2 380 nm). The individual channels and the merged images of the fluorescein and the DIC channels are shown.

labeled with carboxyfluorescein (CF-TL2) on its N-terminus. *S. cerevisiae* and *S. pombe* were incubated in the presence of different peptide concentrations (dark-inactive TL2), but in no case, signs of internal fluorescence were detected, suggesting that cells were unable to take up the peptide or this was quickly extruded (Figure S1). We then proceeded to the enzymatic digestion of the cell wall with lyticase before exposing the cells to the fluorescent peptide. To prevent cell lysis, spheroplasts were maintained in media supplemented with 0.7 M sorbitol for osmotic support. A styryl dye, FM4-64 (16 μM), was used to selectively stain vacuole membranes with red fluorescence.[33] This allowed us to confirm that cell integrity, viability, and endocytic activity were maintained after the spheroplasting process. After co-incubation in the presence of fluorescently labeled and dark-adapted inactive CF-TL2, a specific signal corresponding to the peptide was detected by fluorescence inverted optical microscopy in small cortical patches and bright bigger internal structures, as well as in the vacuole, whose limiting membrane was stained with FM4-64. In addition, a weaker signal in the cytosol was detectable (Figure 2A). The data thus indicated that under these conditions CF-TL2 was most likely internalized into the cells via an endocytic pathway from where it could be translocated into the cytosol. We also analyzed the internalization of the pre-activated CF-TL2 peptide (380 nm) and we compared it to the inactive one (Figure 2B). Like the inactive peptide, the 380 nm-illuminated CF-TL2 accumulates in bright patches at the cortex and at the vacuole, even though the intensity of the fluorescein labeling in the vacuole and the number of cells exhibiting vacuolar staining is significantly lower, as compared to the dark-adapted (inactive) peptide.

TL2 inhibits clathrin-mediated endocytosis in yeast in a light-dependent manner

To investigate the effect of light-activated TL2 on endocytosis, we followed the cortical dynamics of the GFP-tagged coat-associated protein Sla1-GFP. The yeast clathrin adaptor Sla1 is a component of the clathrin coat, whose spatiotemporal dynamics at endocytic sites have been well-characterized.[12,13,34] Spheroplasts of *S. cerevisiae* expressing Sla1-GFP were treated with either pre-activated TL2 (380 nm) or with vehicle, and cortical patches were live-imaged after 30 min incubation. As shown by kymographs generated from 120 s time-lapse movies, light-activated TL2 significantly extended the permanence of the GFP-labelled endocytic patches on the PM (Figure 3A). This effect was dose-, time-, and light-dependent (Figures 3B–3F). Inhibition was observed between 50 and 100 μM and 20–30 min incubation (Figures 3B–3F). As light-induced changes are observable close to the IC_{50} and far from saturating doses,[25] we chose 100 μM and 20 min to quantify light dependency. As reported in mammalian cells,[25] dark-adapted TL2 did not significantly alter CME, thus confirming that the peptide is also constitutively inert in yeast and can stall CME upon UV-induced photoisomerization (Figures 3C and S2). The increase
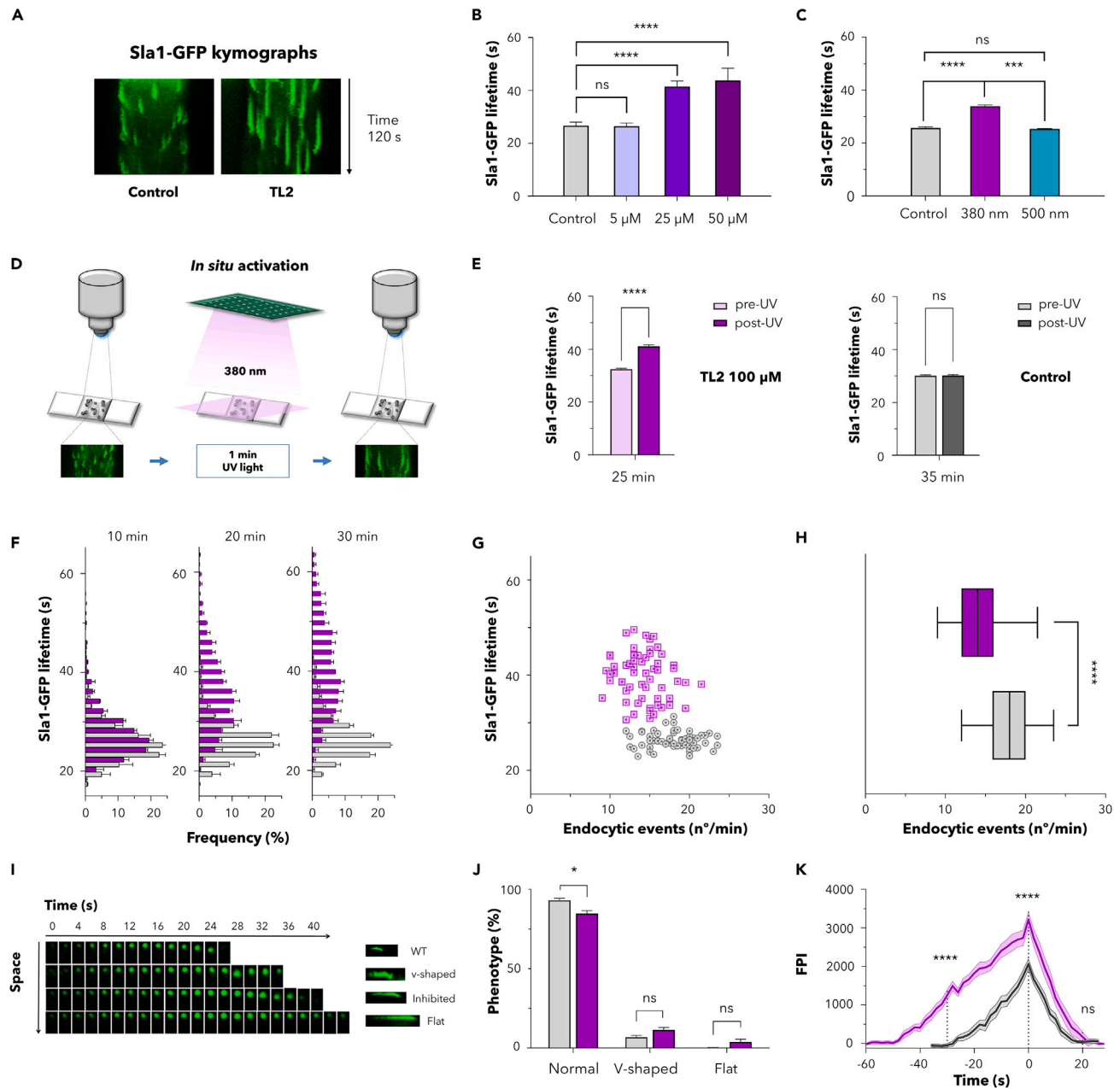
Figure 3. TL2 inhibits CME in yeast in a light-dependent way

(A) Fluorescence kymographs of Sla1-GFP cortical patches from 120 s time-lapse movies of *S. cerevisiae* spheroplasts incubated with 100 μM UV-activated TL2 (illuminated at 380 nm) (right) or mock-treated (left, control).

(B) Mean ± SEM life span of Sla1-GFP cortical patches of yeast spheroplasts either mock-treated (control) or treated with the indicated concentrations of UV-activated TL2 for 30 min.

(C) Mean ± SEM life span of Sla1-GFP cortical patches of yeast either mock-treated (control) or incubated for 20 min with 100 μM of UV-activated TL2 or with the inactive (dark-adapted or illuminated at 500 nm) peptide.

(D) Schematic representation of the protocol used for *in situ* activation experiments. Spheroplasts treated with 100 μM dark-adapted TL2 (inactive) or with vehicle were incubated in parallel for 25 and 35 min, respectively. After that, cortical patches were live imaged in the same group of cells before 380 nm illumination (pre-UV condition) and after 1 min of *in situ* 380 nm illumination (post-UV).

(E) On the left, mean ± SEM life span of Sla1-GFP cortical patches in yeast spheroplasts treated with inactive TL2 (dark-adapted, 100 μM, 25 min) and re-analysed after light-induced activation of the peptide. On the right, mean ± SEM life span of Sla1-GFP cortical patches in yeast spheroplasts mock-treated with vehicle for 35 min and analyzed before and after UV light exposure.

Figure 3. Continued

(F) Graphs showing the progressive change in the lifetime distribution of endocytic Sla1-GFP patches incubated either with vehicle or with pre-activated TL2 (100 μM) for 10, 20, and 30 min. Data are means ± SEM.

(G) Graph showing the TL2 effects on the initiation and maturation of CME sites. Each point represents the average lifespan of cortical Sla1-GFP patches and the number of endocytic *foci* counted per minute in a given cell, 30 min upon incubation with 100 μM UV-activated TL2 (purple) or mock-treated (gray). At least 60 cells from 3 different experiments were analyzed per condition.

(H) Box and whisker (min to max) representation of the number of endocytic events per cell per minute, in cells incubated for 30 min with 100 μM UV-activated TL2 (purple) or mock-treated (gray).

(I) Time-lapse images of Sla1-GFP cortical patches representing the different dynamics observed under our experimental conditions. Patches were defined as wild-type (WT) when internalization and scission occurred within the described average lifetime for Sla1-GFP. Patches that moved inward and then bounced back toward the PM were classified as v-shaped, independently of their life span. Sla1-GFP dynamics were considered delayed when internalization and scission occurred normally, but their cortical life span was extended. Patches were considered flat when no inward movement of the patch was detected.

(J) Frequency plots of patch internalization dynamics, grouped as normal, flat, and v-shaped kymographs (as defined in L), in spheroplasts treated with vehicle or the UV-activated peptide (100 μM, 30 min). Classification refers only to the internalization stage not considering the whole duration of the process. Thus, normal patches include both WT and delayed phenotypes. Data are means ± SEM.

(K) Comparison of the average fluorescence intensity over time traces for cortical Sla1-GFP patches of spheroplasts treated either with vehicle or with pre-activated TL2 (100 μM, 30 min). Traces were aligned on the fluorescence maximum (time 0). Data are mean ± SEM represented by the shading area. A total of 60 patches from 3 different experiments were analyzed per condition. Statistical significance was analyzed at time −30, 0, and 20 s.

Unless differently stated, statistical differences were determined by Student's *t* test (n.s., not significant; *, p value < 0.05; ***, p value < 0.01; ****, p value < 0.001). For B, C, F, and H, at least 200 Sla1-GFP patches in at least 20 different cells were analyzed per condition. For E, at least 100 Sla1-GFP patches in at least 10 different cells were analyzed per condition. All the experiments were repeated at least 3 times and the results were plotted together.

in the Sla1-GFP lifetime could also be observed in *in situ* light-activation experiments where groups of cells treated with inactive TL2 or with vehicle were analyzed before and after exposure to 380 nm UV light for 1 min (Figures 3D and 3E). This demonstrates that TL2 can be activated with light inside the cells.[25]

Subsequently, we focused on characterizing the active isomer (UV-illuminated TL2, 100 μM) and the extent of its activity in *S. cerevisiae* spheroplasts. Live-cell imaging at different incubation times revealed how TL2 progressively delayed Sla1-GFP internalization resulting in both a shift and a broadening of the patches lifetime distribution when compared to vehicle (Figure 3F). The onset of CME inhibition was consistently observed after 20 min, which suggested that the peptide needed to be taken up by endocytosis before translocation to the cytosol. To investigate if clathrin coat assembly, and not only its kinetics, might also be affected by the activated TL2, we quantified both the average Sla1-GFP lifetime, as well as the number of endocytic events per minute. Upon plotting these two parameters for each cell, pre-activated TL2- and vehicle-treated samples distributed into two markedly different populations (Figure 3G). CME inhibition associated with a moderate, but significant reduction in the number of endocytic *foci* (Figure 3H), which were 22% less frequent than in the control. We also investigated if the treatment affected later stages of CME (Figures 3I–3K). In particular, patches were analyzed for their phenotypes and classified according to their internalization patterns (Figure 3I). Normally, the endocytic coat moves into the cytosol as the endocytic invagination grows, and it disassembles as or shortly after the vesicle detaches from the PM. In mutants unable to invaginate the plasma membrane though, the endocytic coat remains at the PM ("flat" phenotype). Finally, in mutants affecting the final scission event an initial inward movement of the coat can be observed, but then it bounces back toward the PM ("v-shaped" phenotype) (Figure 3I).[35–38] TL2-treatment caused marginal changes in the percentage of flat or v-shaped phenotypes compared to vehicle, thus indicating that the peptide does not affect membrane invagination or scission but rather coat maturation and/or cargo loading (Figure 3J). Finally, we analyzed the assembly and disassembly dynamics of the Sla1-GFP cortical patches in cells either mock-treated or treated with activated TL2. Sla1-GFP fluorescence intensity plots as a function of time were aligned at their peak intensity (set as time 0) (Figure 3K). Interestingly, while the assembly and disassembly rates appeared similar in both samples, TL2 produced a very significant increase in the maximum of the fluorescence signal at t = 0, revealing that higher levels of Sla1 are required to sustain endocytic budding or that the coats grow larger in the presence of TL2, before initiating membrane invagination, which is powered by actin polymerization (Figure 3K).[39]

Molecular basis for TL2 activity in yeast

TL2 was designed to interfere with the interaction between β-arrestin and the appendage of the AP2 β-adaptin subunit. However, the yeast AP2 lacks the β2-appendage domain (residues 701–937) that in mammals interacts with the β-arrestin C-terminus and with TL2 through specific residues located in the protein platform subdomain.[25,40] As the yeast α-appendage shares structural similarities with the mammalian β2-appendage, we investigated *in silico* if the former could act as a binding site for our peptide.[26,41] Adaptin-binding motifs occasionally share similar sequences. In particular, an FXXφ hydrophobic core (where φ indicates a hydrophobic residue) is common to both [DE]$_n$X$_{1-2}$[FLI]XX[FL] XXXR and FXXFXXL motifs, which respectively bind the β2-and α-platform subdomains.[26,27,41,42] In both cases, binding is mediated by two hydrophobic sites, which are present in both mammalian appendages, and conserved in *S. cerevisiae*. In yeast, a first hydrophobic interaction might be mediated by F907 (mammalian β2-F837) and by I908 and V954, corresponding to mammalian β2-L838 and β2-A877, respectively. The second hydrophobic interaction might be mediated by W911 (β2-W841) and F972 (β2-Y888). In contrast, clusters of polar residues involved in [DE]$_n$X$_{1-2}$[FLI]XX[FL]XXXR binding are only found in the mammalian β2-subdomain and in the yeast α-appendage.[26,27] In particular, the basic C-terminus of the peptide could interact with E921 and E982 (β2-E849 and β2-E902 in mammalians), whereas its N-terminal acidic region could interact with R956 (β2-R879 and β2-R834 in mammalians) (Figure 4A).
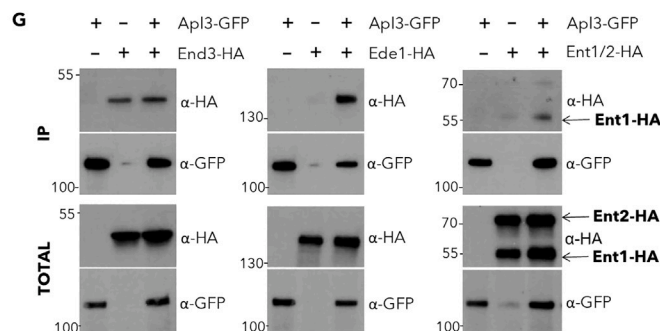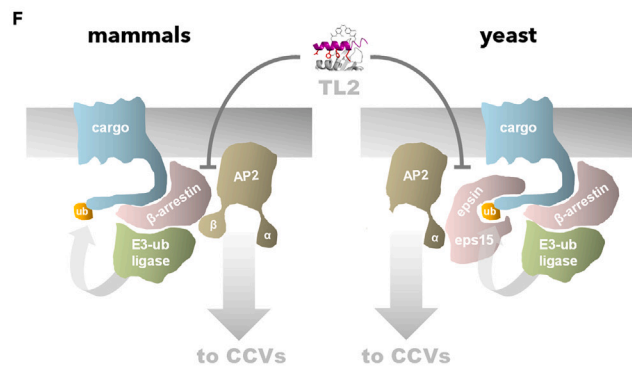
A

AP2B1 human	GK-MERQVFLATWK---DI-PNENELQFQIKEC-HLNA--DT--VS-
AP2A yeast	MHLNLAQ-FISRWKTLSDALG-K-EGEYQ-KSGIKLNK--DFRKVET
AP2A1 human	--MAAQDFFQRWKQLS--LPQ-Q--EAQ-KIF-KANHPMDAE-VTK

AP2B1 human	-SKLQNNNVY---T-IAKR----NVEGQDM----LYQSLKLTNGIWI
AP2A yeast	IS-LEDGLL--LLTQTVKRLGFDIVD-QTSVRSTLFVS-----GI-I
AP2A1 human	A-KLL-GFGSALL---------DNVDPNP----ENFV----GAGI-I

AP2B1 human	LA--E------LRIQPGNP-NYT--LSLKC
AP2A yeast	HTKSEGNFGCLMKIQY--QVNGTVNVTCKT
AP2A1 human	QTKALQV-GCLLRLEPNAQAMYR-LTLRT

B Sla1-GFP kymographs

WT

apl3Δ

Time 120 s

Time 120 s

Control   TL2

C

Sla1-GFP lifetime (s)

WT: **** ; apl3Δ: ns

Control / 100 μM

D

WT / apl3Δ — Endocytic events (n°/min)

Control / 100 μM

E

TL2	DDDIVFECFARQRLCGMKDD
β-arrestin2(380-398)	YATDDDIVFEDFARLRLKG
Epsin1(397-414)	FDTEPD-EFSDFDRLRTAL
Epsin2(451-468)	NGTIKD-DFSEFDNLRTSK
Ent1(364-381)	TGTGID-TFGNVGEARIPA
(92-109)	VLWCRE-NLYIIKTLKEFR
Ent2(448-465)	TGTGID-TFGNTGEARIPA
(92-109)	VLWCRE-NFYVIKTLREFR
Ede1(1019-1037)	QSVRDDDVELPETLEERDTI

F

mammals   TL2   yeast

cargo — AP2 / β-arrestin / E3-ub ligase — to CCVs

G

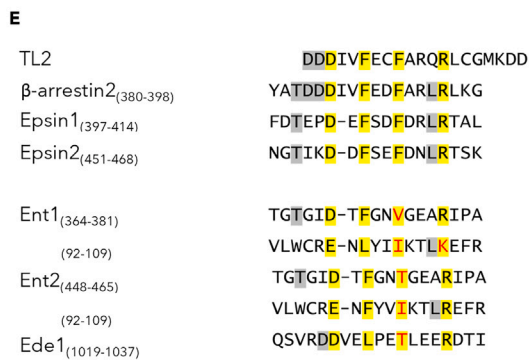IP / TOTAL: α-HA, α-GFP blots
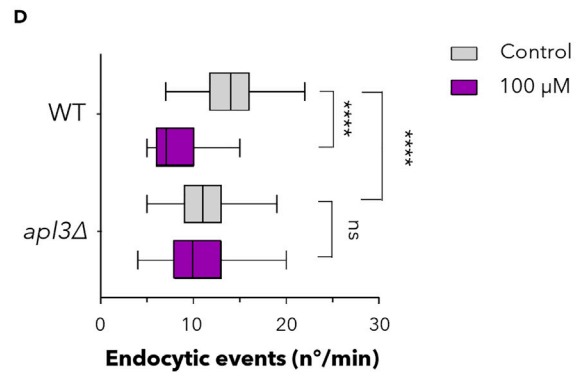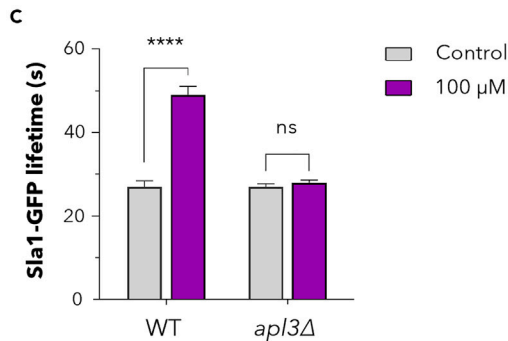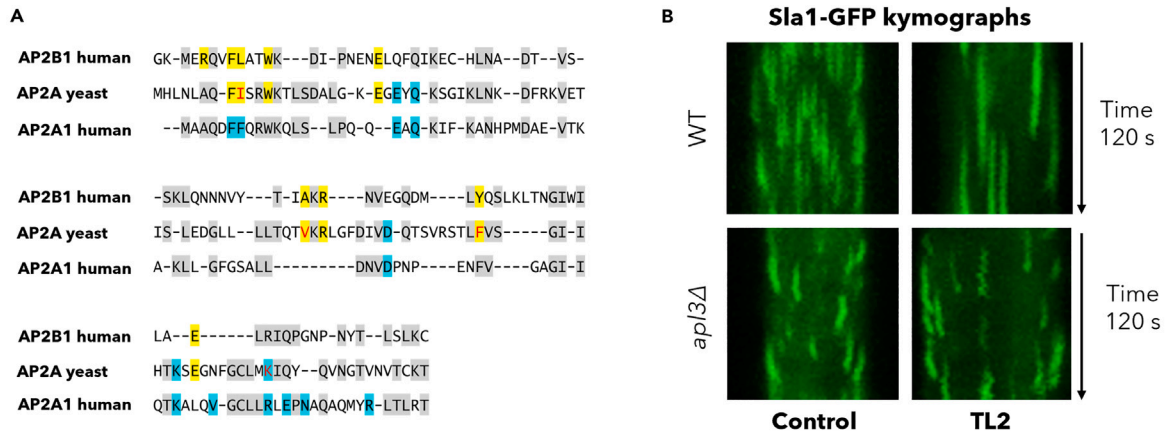
Apl3-GFP / End3-HA / Ede1-HA / Ent1/2-HA

Figure 4. Light-activated TL2 targets α-adaptin in *S. cerevisiae*

(A) Sequence alignment between the human β2-appendage, and the human and yeast α-appendage platform subdomains from AP2. Residues binding to the TL2 interaction motif [DE]$_n$X$_{1-2}$[FLI]XX[FL]XXXR are highlighted in yellow, conserved substitutions in red. Residues marked in cyan mediate binding to cargo adaptors in the human α-appendage. Additional conserved residues between the three domains are pictured in gray.

(B) Fluorescence kymographs of Sla1-GFP cortical patches from 120 s time-lapse movies of the indicated *S. cerevisiae* strain spheroplasts incubated with 100 μM UV-activated TL2 (illuminated at 380 nm) (right) or mock-treated (control, left).

(C) Mean ± SEM life span of Sla1-GFP cortical patches of spheroplasts of the indicated yeast strains either mock-treated (control, gray) or treated for 20 min with 100 μM of UV-activated TL2 (purple). n > 50 patches per condition.

(D) Box and whisker (min to max) representation of the number of endocytic events per cell per minute, in cells incubated for 20 min with 100 μM UV-activated TL2 (purple) or mock-treated (gray). n = 50 cells per condition.

(E) The AP2 interaction motif [DE]$_n$X$_{1-2}$[FLI]XX[FL]XXXR in TL2, human β-arrestin2 and epsins, and possible conserved motifs from the yeast epsin homologues, Ent1 and Ent2, and the Eps15 homology (EH) domain-containing protein Ede1. Hotspots mediating binding to AP2 are highlighted in yellow. Residues in red are conservative substitutions between the mammalian and yeast proteins. Further conserved residues are highlighted in gray.

(F) Diagram representing the proposed interactions altered by UV-activated TL2 in mammals and yeast.

(G) Immunoblots of anti-GFP agarose precipitates (IP (GFP)) from yeast expressing the indicated GFP and/or HA-tagged proteins (+) or non-tagged (−), either probed for HA (α-HA) or GFP (α-GFP). 10 μg of total protein were loaded for the inputs.

Unless differently stated, statistical differences were determined by Student's *t* test (n.s., not significant; *, p value < 0.05; ***, p value < 0.01; ****, p value < 0.001).

Light-activated TL2 targets α-adaptin in *S. cerevisiae* and unveils a conserved function of AP2 in yeast

To investigate if TL2 interferes with CME by interacting with the α-adaptin subunit, we tested the activity of UV-activated TL2 in a strain background lacking the gene *APL3*, encoding that subunit. To that end, WT and *apl3Δ* strains expressing genome-edited Sla1-GFP were treated for 20 min with 100 μM of UV-activated TL2 or vehicle. The life span of cortical Sla1-GFP patches and the number of endocytic events per minute were then investigated by live-cell fluorescence microscopy. UV-activated TL2 again significantly diminished the number of endocytic events per minute and elongated the cortical life span of Sla1-GFP in WT cells, but it was completely inactive in the *apl3Δ* background under the same experimental conditions (Figures 4B–4D). This result demonstrates that AP2 is the relevant target of UV-activated TL2 in yeast.

Arrestin-like proteins (ARTs) exist in yeast, and, similarly to mammalian arrestins, they act as E3 ubiquitin ligase cargo adaptor.[38] Unlike mammalian arrestins though, yeast ARTs lack the specific residues that mediate binding to AP2 and clathrin.[43–45] Interestingly, the yeast epsins Ent1 and Ent2, and the Eps15 homology (EH) domain–containing proteins Ede1 and End3, some of which work as clathrin adaptors for ubiquitinated cargo,[46] bear sequences similar to the [DE]$_n$X$_{1-2}$[FLI]XX[FL]XXXR AP2-binding motif, present in mammalian β-arrestins, epsins, and in the TL2 peptide (Figure 4E). Therefore, the mammalian arrestin functions as E3-ubiquitin ligase and clathrin adaptor might be split in yeast, and TL2 might then interfere with the clathrin adaptor function, rather than with the ARTs (Figure 4F).

Consistent with this hypothesis, we could demonstrate the yeast α-adaptin (Apl3) specifically interacted with Ede1 in immunoprecipitation experiments using genome-edited strains to express Apl3-GFP and/or Ede1-HA fusion proteins (Figure 4G). A functionally relevant interaction of Eps15 family members with the α-appendage domain was previously described in mammalian cells.[41,47] Weaker binding of the yeast α-adaptin to the epsin Ent1 could be detected as well in similar experiments, but not with Ent2 or End3 (Figure 4G).

DISCUSSION

We have shown that the photoswitchable peptide TL2 designed from the sequence and structure of the human β-arrestin C-terminus can be effectively used to photocontrol CME in yeast. As observed in mammalian cells, TL2 could cross the yeast membranes in minutes, most likely via a mechanism requiring endocytic internalization to reach an acidic environment. After 20 min, TL2 accumulated at concentrations sufficient to inhibit CME. We demonstrated that pre-illuminated (*cis*, helical) TL2 bound to its target in a conformation that reduced the frequency of endocytic events and increased their duration, and thus, it interfered with clathrin-coated pit (CCP) nucleation or stabilization and also with endocytic coat maturation. The *trans*, less helical peptide appeared inactive under the same experimental conditions, but could be activated *in situ* by exposing TL2-treated spheroplasts to UV light.

In this work, we also demonstrate that the relevant TL2 target in yeast is the α-adaptin subunit of the AP2 complex, since the deletion of this subunit renders yeast completely insensitive to UV-activated TL2. Interestingly, as previously reported for other constitutive knock-out strains of the AP2 complex subunits,[30,31] we did not detect changes in the life span of the endocytic coat and only a slight drop in the number of endocytic events per minute in the *apl3Δ* strain, as compared to the WT in the absence of the peptide. Instead, pharmacological inhibition of AP2 function with TL2 significantly diminished the number of endocytic events and interfered with coat maturation in the WT. Those phenotypes have been described upon the depletion of AP2 in mammalian cells by siRNA,[48] indicating that AP2 actually has a conserved endocytic function in yeast, which is masked by compensatory mechanisms upon the constitutive depletion of the complex. Importantly, compensatory mechanisms have also been observed for clathrin mutants in *S. cerevisiae*.[49]

In addition, our *in silico* and experimental data identified Apl3 molecular interactors that might explain both the endocytic coat nucleation and maturation defects observed in the presence of the activated peptide, namely, Ede1 and Ent1. Ede1 and Ent1 both bear the consensus AP2 binding motif present in TL2, and specifically immunoprecipitated with Apl3. Ede1, similar to the AP2 complex, arrives early at endocytic sites and its depletion causes a drop in the number of endocytic events per minute, as observed upon TL2 treatment.[30,50] However, the depletion of Ede1 shortens the Sla1-GFP life span,[30,50] as opposed to TL2 treatment. On the contrary, and similar to TL2 treatment, mutations in Ent1 extend the lifespan of Sla1-GFP.[46,51] Ent1, interacts with Ede1 through their NPF motif and EH domains, respectively, but it arrives later at

endocytic sites, where it is proposed to hook ubiquitinated cargo and the clathrin coat to the endocytic actin scaffold.[30,51] Thus, simultaneous and specific inhibition of Ede1 and Ent1 interaction with AP2 rendered a phenotype that is not fully recapitulated by the deletion of any of the genes involved, but rather, it combines some of their features. Our results strongly indicate that AP2 might work as a hinge stabilizing the early endocytic scaffolds through its interaction with Ede1, and regulate progression to endocytic budding through the recruitment of Ent1, maybe in response to cargo loading.[52]

Thus, light-activated TL2 allowed us to assess the effect of specifically interfering with the $[DE]_nX_{1-2}[FLI]XX[FL]XXLR$ motif on several endocytic proteins and it resulted in a combination of phenotypes otherwise only appreciable by performing time-consuming, multiple conditional point mutations.

Limitations of the study

Although TL2 allows for the first time to inhibit CME in yeast, its molecular properties impose certain experimental limitations to use it. While yeast are easy to handle, spheroplasts are fragile and prone to osmotic lysis because of their missing cell wall. The requirements of long incubations followed by extended imaging and UV light exposure proved to be stressful conditions and prevented us from studying in spheroplasts the reversibility of TL2 activation under several cycles of illumination. This limitation could be partially overcome by synthesizing a TL2 analogue with visible or infrared activation wavelength,[53,54] whose lower excitation energy would allow milder experimental conditions. Finally, TL2 was specifically designed to target the interaction between human β-arrestin and AP2 β-adaptin. An optimized sequence based on the proposed interactions in yeast would grant higher pharmacological potency thereby allowing to use lower concentrations of peptide in the spheroplast medium.

Conclusion

In summary, we have characterized the TL2 activity in *S. cerevisiae* spheroplasts, and we have proved that its ability to control CME with light spans throughout evolution. We also demonstrate that the relevant target of TL2 in yeast is the AP2 complex, thus unveiling conserved functions for this clathrin adaptor that were previously unnoticed in constitutive knock-out backgrounds, possibly due to compensatory effects. Further, we identified functionally relevant endocytic proteins bearing the $[DE]_nX_{1-2}[FLI]XX[FL]XXLR$ motif present in TL2, whose altered interaction with the α-adaptin appendage can explain the phenotypes installed in the presence of the activated peptide. Finally, our data indicate that conserved endocytic functions such as cargo loading can be executed by conserved molecular interfaces, regardless of the particular proteins that offer those. To the best of our knowledge, no other means to achieve specific pharmacological inhibition of CME have been described in yeast. Other drugs previously used, such as filipin or Latrunculin A, have many pleiotropic effects and cannot be spatially controlled. Thus, TL2 offers a tool to spatiotemporal control endocytosis at will with subcellular resolution, allowing studies on the relevance of the dynamic architecture of CME in a myriad of cellular processes such as cytokinesis of polarized growth.

STAR★METHODS

Detailed methods are provided in the online version of this paper and include the following:

- KEY RESOURCES TABLE
- RESOURCE AVAILABILITY
  - Lead contact
  - Materials availability
  - Data and code availability
- EXPERIMENTAL MODEL AND STUDY PARTICIPANT DETAILS
  - Yeast strains
- METHOD DETAILS
  - Synthesis of the photoswitchable crosslinker (BSBCA)
  - TL2 crosslinking procedure
  - Peptide isolation
  - TL2 analytical characterization
  - Peptide quantification
  - Yeast growth conditions
  - Peptide uptake in yeast
  - *S. Cerevisiae* spheroplasts preparation
  - Peptide uptake in spheroplasts
  - Cortical patch dynamics
  - Fluorescence microscopy
  - Immunoprecipitation and immunoblots
- QUANTIFICATION AND STATISTICAL ANALYSIS

SUPPLEMENTAL INFORMATION

ACKNOWLEDGMENTS

AUTHOR CONTRIBUTIONS

Conceptualization and supervision of the project, P.G. and M.I.G.; experimental design, D.P., J.E.D., E.R., M.I.G., and P.G.; experimental work, D.P., N.C., M.C.P., and L.P.; data analysis, D.P., M.C.P., J.P., N.C., and M.I.G.; chemical synthesis and purification, D.P., A.M.Q., L.N., and E.G.; writing - original draft, D.P., P.G., and M.I.G.; writing – review and editing, D.P., N.C., P.G., and M.I.G.

DECLARATION OF INTERESTS

The authors declare no competing interests.

INCLUSION AND DIVERSITY

We support inclusive, diverse, and equitable conduct of research.

REFERENCES

1. Papatheodorou, P., Zamboglou, C., Genisyuerek, S., Guttenberg, G., and Aktories, K. (2010). Clostridial glucosylating toxins enter cells via clathrin-mediated endocytosis. PLoS One 5, e10673. https://doi.org/10.1371/journal.pone.0010673.

2. Abrami, L., Liu, S., Cosson, P., Leppla, S.H., and Van der Goot, F.G. (2003). Anthrax toxin triggers endocytosis of its receptor via a lipid raft-mediated clathrin-dependent process. J. Cell Biol. 160, 321–328. https://doi.org/10.1083/jcb.200211018.

3. Deinhardt, K., Berninghausen, O., Willison, H.J., Hopkins, C.R., and Schiavo, G. (2006). Tetanus toxin is internalized by a sequential clathrin-dependent mechanism initiated within lipid microdomains and independent of epsin 1. J. Cell Biol. 174, 459–471. https://doi.org/10.1083/jcb.200508170.

4. Veiga, E., and Cossart, P. (2006). The role of clathrin-dependent endocytosis in bacterial internalization. Trends Cell Biol. 16, 499–504. https://doi.org/10.1016/j.tcb.2006.08.005.

5. Cossart, P., and Helenius, A. (2014). Endocytosis of viruses and bacteria. Cold Spring Harbor Perspect. Biol. 6, a016972. https://doi.org/10.1101/cshperspect.a016972.

6. Inoue, Y., Tanaka, N., Tanaka, Y., Inoue, S., Morita, K., Zhuang, M., Hattori, T., and Sugamura, K. (2007). Clathrin-Dependent Entry of Severe Acute Respiratory Syndrome Coronavirus into Target Cells Expressing ACE2 with the Cytoplasmic Tail Deleted. J. Virol. 81, 8722–8729. https://doi.org/10.1128/jvi.00253-07.

7. Bayati, A., Kumar, R., Francis, V., and McPherson, P.S. (2020). SARS-CoV-2 infects cells following viral entry via clathrin-mediated endocytosis. Preprint at bioRxiv. https://doi.org/10.1101/2020.07.13.201509.

8. McMahon, H.T., and Boucrot, E. (2011). Molecular mechanism and physiological functions of clathrin-mediated endocytosis. Nat. Rev. Mol. Cell Biol. 12, 517–533. https://doi.org/10.1038/nrm3151.

9. Boettner, D.R., Chi, R.J., and Lemmon, S.K. (2011). Lessons from yeast for clathrin-mediated endocytosis. Nat. Cell Biol. 14, 2–10. https://doi.org/10.1038/ncb2403.

10. Weinberg, J., and Drubin, D.G. (2012). Clathrin-mediated endocytosis in budding yeast. Trends Cell Biol. 22, 1–13. https://doi.org/10.1016/j.tcb.2011.09.001.

11. Kaksonen, M., and Roux, A. (2018). Mechanisms of clathrin-mediated endocytosis. Nat. Rev. Mol. Cell Biol. 19, 313–326. https://doi.org/10.1038/nrm.2017.132.

12. Kaksonen, M., Sun, Y., and Drubin, D.G. (2003). A Pathway for association of receptors, adaptors, and actin during endocytic internalization. Cell 115, 475–487.

13. Kaksonen, M., Toret, C.P., and Drubin, D.G. (2005). A modular design for the clathrin- and actin-mediated endocytosis machinery. Cell 123, 305–320. https://doi.org/10.1016/j.cell.2005.09.024.

14. Idrissi, F.Z., Grötsch, H., Fernández-Golbano, I.M., Presciatto-Baschong, C., Riezman, H., and Geli, M.I. (2008). Distinct acto/myosin-I structures associate with endocytic profiles at the plasma membrane. J. Cell Biol. 180, 1219–1232. https://doi.org/10.1083/jcb.200708060.

15. Idrissi, F.Z., Blasco, A., Espinal, A., and Geli, M.I. (2012). Ultrastructural dynamics of proteins involved in endocytic budding. Proc. Natl. Acad. Sci. USA 109, E2587–E2594. https://doi.org/10.1073/pnas.1202789109.

16. Kukulski, W., Schorb, M., Welsch, S., Picco, A., Kaksonen, M., and Briggs, J.A.G. (2011). Correlated fluorescence and 3D electron microscopy with high sensitivity and spatial precision. J. Cell Biol. 192, 111–119. https://doi.org/10.1083/jcb.201009037.

17. Kukulski, W., Schorb, M., Kaksonen, M., and Briggs, J.A.G. (2012). Plasma Membrane Reshaping during Endocytosis Is Revealed by Time-Resolved Electron Tomography. Cell 150, 508–520. https://doi.org/10.1016/j.cell.2012.05.046.

18. von Kleist, L., and Haucke, V. (2012). At the Crossroads of Chemistry and Cell Biology: Inhibiting Membrane Traffic by Small Molecules. Traffic 13, 495–504. https://doi.org/10.1111/j.1600-0854.2011.01292.x.

19. Mishev, K., Dejonghe, W., and Russinova, E. (2013). Small molecules for dissecting endomembrane trafficking: A cross-systems view. Chem. Biol. 20, 475–486. https://doi.org/10.1016/j.chembiol.2013.03.009.

20. Ayscough, K.R., Stryker, J., Pokala, N., Sanders, M., Crews, P., and Drubin, D.G. (1997). High rates of actin filament turnover in budding yeast and roles for actin in establishment and maintenance of cell polarity revealed using the actin inhibitor latrunculin-A. J. Cell Biol. 137, 399–416. https://doi.org/10.1083/jcb.137.2.399.

21. Encinar del Dedo, J., Idrissi, F.Z., Fernandez-Golbano, I.M., Garcia, P., Rebollo, E., Krzyzanowski, M.K., Grötsch, H., and Geli, M.I. (2017). ORP-Mediated ER Contact with Endocytic Sites Facilitates Actin Polymerization. Dev. Cell 43, 588–602.e6. https://doi.org/10.1016/j.devcel.2017.10.031.

22. Dutta, D., and Donaldson, J.G. (2012). Search for inhibitors of endocytosis. Cell. Logist. 2, 203–208. https://doi.org/10.4161/cl.23967.

23. Elkin, S.R., Oswald, N.W., Reed, D.K., Mettlen, M., MacMillan, J.B., and Schmid, S.L. (2016). Ikarugamycin: A Natural Product Inhibitor of Clathrin-Mediated Endocytosis. Traffic 17, 1139–1149. https://doi.org/10.1111/tra.12425.

24. Dejonghe, W., Sharma, I., Denoo, B., De Munck, S., Lu, Q., Mishev, K., Bulut, H., Mylle, E., De Rycke, R., Vasileva, M., et al. (2019). Disruption of endocytosis through chemical inhibition of clathrin heavy chain function. Nat. Chem. Biol. 15, 641–649. https://doi.org/10.1038/s41589-019-0262-1.

25. Nevola, L., Martín-Quirós, A., Eckelt, K., Camarero, N., Tosi, S., Llobet, A., Giralt, E., and Gorostiza, P. (2013). Light-regulated stapled peptides to inhibit protein-protein interactions involved in clathrin-mediated endocytosis. Angew. Chem., Int. Ed. Engl. 52, 7704–7708. https://doi.org/10.1002/anie.201303324.

26. Schmid, E.M., Ford, M.G.J., Burtey, A., Praefcke, G.J.K., Peak-Chew, S.Y., Mills, I.G., Benmerah, A., and McMahon, H.T. (2006). Role of the AP2 β-appendage hub in recruiting partners for clathrin-coated vesicle assembly. PLoS Biol. 4, e262–e1548. https://doi.org/10.1371/journal.pbio.0040262.

27. Edeling, M.A., Mishra, S.K., Keyel, P.A., Steinhauser, A.L., Collins, B.M., Roth, R., Heuser, J.E., Owen, D.J., and Traub, L.M. (2006). Molecular switches involving the AP-2 β2 appendage regulate endocytic cargo selection and clathrin coat assembly. Dev. Cell 10, 329–342. https://doi.org/10.1016/j.devcel.2006.01.016.

28. Zhang, Z., Burns, D.C., Kumita, J.R., Smart, O.S., and Woolley, G.A. (2003). A water-soluble azobenzene cross-linker for photocontrol of peptide conformation. Bioconjugate Chem. 14, 824–829. https://doi.org/10.1021/bc0340161.

29. Martín-Quirós, A., Nevola, L., Eckelt, K., Madurga, S., Gorostiza, P., and Giralt, E. (2015). Absence of a stable secondary structure is not a limitation for photoswitchable inhibitors of β-arrestin/β-adaptin 2 protein-protein interaction. Chem. Biol. 22, 31–37. https://doi.org/10.1016/j.chembiol.2014.10.022.

30. Kaksonen, M., Toret, C.P., and Drubin, D.G. (2005). A modular design for the clathrin- and actin-mediated endocytosis machinery. Cell 123, 305–320. https://doi.org/10.1016/j.cell.2005.09.024.

31. Huang, K.M., D'Hondt, K., Riezman, H., and Lemmon, S.K. (1999). Clathrin functions in the absence of heterotetrameric adaptors and AP180-related proteins in yeast. EMBO J. 18, 3897–3908. https://doi.org/10.1093/emboj/18.14.3897.

32. Parenteau, J., Klinck, R., Good, L., Langel, Ü., Wellinger, R.J., and Elela, S.A. (2005). Free uptake of cell-penetrating peptides by fission yeast. FEBS Lett. 579, 4873–4878. https://doi.org/10.1016/j.febslet.2005.07.064.

33. Vida, T.A., and Emr, S.D. (1995). A new vital stain for visualizing vacuolar membrane dynamics and endocytosis in yeast. J. Cell Biol. 128, 779–792.

34. Tolsma, T.O., Cuevas, L.M., and Di Pietro, S.M. (2018). The Sla1 adaptor-clathrin interaction regulates coat formation and progression of endocytosis. Traffic 19, 446–462. https://doi.org/10.1111/tra.12563.

35. Arasada, R., and Pollard, T.D. (2011). Distinct roles for F-BAR proteins Cdc15p and Bzz1p in actin polymerization at sites of endocytosis in fission yeast. Curr. Biol. 21, 1450–1459. https://doi.org/10.1016/j.cub.2011.07.046.

36. Basu, R., and Chang, F. (2011). Characterization of dip1p reveals a switch in Arp2/3-dependent actin assembly for fission yeast endocytosis. Curr. Biol. 21, 905–916. https://doi.org/10.1016/j.cub.2011.04.047.

37. Kishimoto, T., Sun, Y., Buser, C., Liu, J., Michelot, A., and Drubin, D.G. (2011). Determinants of endocytic membrane geometry, stability, and scission. Proc. Natl. Acad. Sci. USA 108, E979–E988. https://doi.org/10.1073/pnas.1113413108.

38. Aghamohammadzadeh, S., Smaczynska-de Rooij, I.I., and Ayscough, K.R. (2014). An Abp1-dependent route of endocytosis functions when the classical endocytic pathway in yeast is inhibited. PLoS One 9, 1–11. https://doi.org/10.1371/journal.pone.0103311.

39. Kaksonen, M., Sun, Y., and Drubin, D.G. (2003). A Pathway for Association of Receptors, Adaptors, and Actin during Endocytic Internalization. Cell 115, 475–487. https://doi.org/10.1016/S0092-8674(03)00883-3.

40. Chapa-y-Lazo, B., Allwood, E.G., Smaczynska-de Rooij, I.I., Snape, M.L., and Ayscough, K.R. (2014). Yeast endocytic adaptor AP-2 binds the stress sensor Mid2 and functions in polarized cell responses. Traffic 15, 546–557. https://doi.org/10.1111/tra.12155.

41. Praefcke, G.J.K., Ford, M.G.J., Schmid, E.M., Olesen, L.E., Gallop, J.L., Peak-Chew, S.Y., Vallis, Y., Babu, M.M., Mills, I.G., and McMahon, H.T. (2004). Evolving nature of the AP2 α-appendage hub during clathrin-coated vesicle endocytosis. EMBO J. 23, 4371–4383. https://doi.org/10.1038/sj.emboj.7600445.

42. Olesen, L.E., Ford, M.G.J., Schmid, E.M., Vallis, Y., Babu, M.M., Li, P.H., Mills, I.G., McMahon, H.T., and Praefcke, G.J.K. (2008). Solitary and repetitive binding motifs for the AP2 complex α-appendage in amphiphysin and other accessory proteins. J. Biol. Chem. 283, 5099–5109. https://doi.org/10.1074/jbc.M708621200.

43. Moore, C.A.C., Milano, S.K., and Benovic, J.L. (2007). Regulation of receptor trafficking by GRKs and arrestins. Annu. Rev. Physiol. 69, 451–482. https://doi.org/10.1146/annurev.physiol.69.022405.154712.

44. Lin, C.H., MacGurn, J.A., Chu, T., Stefan, C.J., and Emr, S.D. (2008). Arrestin-Related Ubiquitin-Ligase Adaptors Regulate Endocytosis and Protein Turnover at the Cell Surface. Cell 135, 714–725. https://doi.org/10.1016/j.cell.2008.09.025.

45. Myers, M.D., and Payne, G.S. (2013). Clathrin adaptors and disease: Insights from the yeast Saccharomyces cerevisiae. Front. Biosci. 18, 862–891. https://doi.org/10.2741/4149.

46. Maldonado-Báez, L., Dores, M.R., Perkins, E.M., Drivas, T.G., Hicke, L., and Wendland, B. (2008). Interaction between epsin/yap180 adaptors and the scaffolds Ede1/Pan1 is required for endocytosis. Mol. Biol. Cell 19, 2936–2948. https://doi.org/10.1091/mbc.E07-10-1019.

47. Benmerah, A., Lamaze, C., Bègue, B., Schmid, S.L., Dautry-Varsat, A., and Cerf-Bensussan, N. (1998). Ap-2/Eps15 interaction is required for receptor-mediated endocytosis. J. Cell Biol. 140, 1055–1062. https://doi.org/10.1083/jcb.140.5.1055.

48. Boucrot, E., Saffarian, S., Zhang, R., and Kirchhausen, T. (2010). Roles of AP-2 in clathrin-mediated endocytosis. PLoS One 5, e10597. https://doi.org/10.1371/journal.pone.0010597.

49. Lemmon, S.K., and Jones, E.W. (1987). Clathrin requirement for normal growth of yeast. Science 238, 504–509. https://doi.org/10.1126/science.3116672.

50. Stimpson, H.E.M., Toret, C.P., Cheng, A.T., Pauly, B.S., and Drubin, D.G. (2009). Early-arriving Syp1p and Ede1p function in endocytic site placement and formation in budding yeast. Mol. Biol. Cell 20, 4640–4651. https://doi.org/10.1091/mbc.E09-05-0429.

51. Skruzny, M., Desfosses, A., Prinz, S., Dodonova, S.O., Gieras, A., Uetrecht, C., Jakobi, A.J., Abella, M., Hagen, W.J.H., Schulz, J., et al. (2015). An Organized Co-assembly of Clathrin Adaptors Is Essential for Endocytosis. Dev. Cell 33, 150–162. https://doi.org/10.1016/j.devcel.2015.02.023.

52. Carroll, S.Y., Stimpson, H.E.M., Weinberg, J., Toret, C.P., Sun, Y., and Drubin, D.G. (2012). Analysis of yeast endocytic site formation and maturation through a regulatory transition point. Mol. Biol. Cell 23, 657–668. https://doi.org/10.1091/mbc.E11-02-0108.

53. Cabré, G., Garrido-Charles, A., Moreno, M., Bosch, M., Porta-de-la-Riva, M., Krieg, M., Gascón-Moya, M., Camarero, N., Gelabert, R., Lluch, J.M., et al. (2019). Rationally designed azobenzene photoswitches for efficient two-photon neuronal excitation. Nat. Commun. 10, 907. https://doi.org/10.1038/s41467-019-08796-9.

54. Chi, I., Sadovski, O., and Woolley, G.A. (2006). A blue-green absorbing cross-linker for rapid photoswitching of peptide helix content. Bioconjugate Chem. 17, 670–676. https://doi.org/10.1021/bc050363u.

55. Fernández-Golbano, I.M., Idrissi, F.Z., Giblin, J.P., Grosshans, B.L., Robles, V., Grötsch, H., Borrás, M.delM., and Geli, M.I. (2014). Crosstalk between PI(4,5)P2 and CK2 modulates actin polymerization during endocytic uptake. Dev. Cell 30, 746–758. https://doi.org/10.1016/j.devcel.2014.07.020.

56. Longtine, M.S., McKenzie, A., 3rd, Demarini, D.J., Shah, N.G., Wach, A., Brachat, A., Philippsen, P., and Pringle, J.R. (1998). Additional modules for versatile and economical PCR-based gene deletion and modification in Saccharomyces cerevisiae. Yeast 14, 953–961. https://doi.org/10.1002/(SICI)1097-0061(199807)14:10<953::AID-YEA293>3.0.CO;2-U.

57. Wach, A., Brachat, A., Alberti-Segui, C., Rebischung, C., and Philippsen, P. (1997). Heterologous HIS3 marker and GFP reporter modules for PCR-targeting in Saccharomyces cerevisiae. Yeast *13*. https://doi.org/10.1002/(SICI)1097-0061(19970915)13:11<1065::AID-YEA159>3.0.CO;2-K.

58. Burns, D.C., Zhang, F., and Woolley, G.A. (2007). Synthesis of 3,3'-bis(sulfonato)-4,4'-bis(chloroacetamido) azobenzene and cysteine cross-linking for photo-control of protein conformation and activity. Nat. Protoc. *2*, 251–258. https://doi.org/10.1038/nprot.2007.21.

59. Laemmli, U.K. (1970). Cleavage of structural proteins during the assembly of the head of bacteriophage T4. Nature *227*, 680–685.

60. Schneider, C.A., Rasband, W.S., and Eliceiri, K.W. (2012). NIH Image to ImageJ: 25 years of image analysis. Nat. Methods *9*, 671–675. https://doi.org/10.1038/nmeth.2089.

STAR★METHODS

KEY RESOURCES TABLE

REAGENT or RESOURCE	SOURCE	IDENTIFIER
Antibodies		
Anti-HA-Peroxidase, High Affinity from rat IgG$_1$	Roche	Cat# 12013819001; RRID: AB_390917
Anti-GFP monoclonal antibody (JL-8)	Clontech	Cat# 632381; RRID: AB_2313808
Goat anti-mouse antibody conjugated to horseradish peroxidase (HRP)	Merck	Cat# A2554; RRID: AB_258008
Chemicals, peptides, and recombinant proteins		
Vent® DNA Polymerase	BioLabs	M0254S
2,5-diaminobenzenesulfonic acid (≥97%)	Sigma-Aldrich	Cat#32776
Acetic acid, glacial (ACS reagent, ≥99.7%)	Sigma-Aldrich	Cat#695092
Acetic anhydride (*ReagentPlus*®, ≥99%)	Sigma-Aldrich	Cat#320102
Sodium carbonate (powder, ≥99.5%, ACS reagent)	Sigma-Aldrich	Cat#223530
Sodium hypochlorite solution (min. 14% free chlorine)	Fisher Chemical	Cat#10691164
NaOH (pellets, ACS reagent, ≥97.0%)	Sigma-Aldrich	Cat#221465
Chloroacetic acid (ACS reagent, ≥99.0%)	Sigma-Aldrich	Cat#402923
Chloroacetic anhydride (95%)	Sigma-Aldrich	Cat#215163
Trizma® base (puriss. p.a., ≥99.7%)	Sigma-Aldrich	Cat#93350
Tris-(2-carboxyethyl)phosphine (0.5 M, pH 7.0)	Sigma-Aldrich	Cat#646547
TL2 peptide (uncrosslinked), 5 mg, purity >85%	Ontores Biotechnologies Inc.	Custom synthesis
2-mercaptoethanol (BioUltra, ≥99.0%)	Sigma-Aldrich	Cat#63689
Lyticase from *Arthrobacter luteus* (lyophilized powder, ≥2,000 units/mg protein)	Sigma-Aldrich	Cat#L2524
D-Sorbitol (BioReagent)	Sigma-Aldrich	Cat#S3889
FM™ 4–64 Dye	Molecular Probes (Invitrogen)	Cat#T13320
Phenylmethanesulfonyl fluoride (PMSF)	Sigma-Aldrich	Cat#P7626
Leupeptin	Roche Diagnostics GmbH	Cat#11017128001
Antipain	Roche Diagnostics GmbH	Cat#11004646001
Pepstatin	Roche Diagnostics GmbH	Cat#11359053001
Aprotinin	Roche Diagnostics GmbH	Cat#1023662401
ChromoTek GFP-Trap®Agarose	Proteintech	Cat#gta
Protran BA85 nitrocellulose membranes	Amersham	Cat#10600002
Critical commercial assays		
ECL kit	Amersham	Cat#RPN2209
Mini-PROTEAN TGX 4-20% Acrylamide gels	BioRad	Cat#4561096
Experimental models: Organisms/strains		
h^{90} leu1-32 ura4-Δ18 his3-d1	F. Azorín (IBMB-CSIC)	SpA64
Mata his3 leu2 met15 ura3	Euroscarf	SCMIG381
Mata his3 leu2 ura3 trp1 SLA1-GFP::TRP1	Fernández-Golbano et al.[55]	SCMIG933
Mata his3 leu2 met15 ura3 apl3Δ::kanMX4 SLA1-GFP::HIS3MX	This study	SCMIG1607
Matα his3 leu2 lys2 ura3 APL3-GFP::HIS3MX	This study	SCMIG1610
Mata his3 leu2 ura3 trp1 bar1-1 EDE1-3HA::TRP1	This study	SCMIG1213
Mata his3 leu2 met15 ura3 END3-3HA::HIS3	This study	SCMIG1608

Continued

REAGENT or RESOURCE	SOURCE	IDENTIFIER
Mata his3 leu2 ura3 trp1 bar1-1 ENT1-3HA::TRP1 ENT2-3HA::HIS3MX	This study	*SCMIG1214*
Mata his3 leu2 trp1 ura3 bar1-1 EDE1-3HA::TRP1 APL3-GFP::HIS3	This study	*SCMIG1612*
Mata his3 leu2 met15 ura3 END3-3HA::HIS3 APL3-GFP::KMX	This study	*SCMIG1613*
Mata/Matα his3/his3 leu2/leu2 ura3/ura3 trp1/TRP1 LYS2/lys2 bar1-1/BAR1 ENT1-3HA::TRP1/ENT1 ENT2-3HA::HIS3MX/ENT2 APL3/APL3-GFP::HIS3MX	This study	*SCMIG1618*
Oligonucleotides		
GAAGTACATTGTCGAATGTATAAAGAATGT GCTTACGAAGCGGATCCCCGGGTTAATTAA	This study	APL3.F2
CAATGCGGATGATTTTCATTATAGTGAATTT GAGAAAATTGAATTCGAGCTCGTTTAAAC	This study	APL3.R1
GGATCTAGAAGCCGCCACTAACTTTTTGTT GGATAGTGCTCGGATCCCCGGGTTAATTAA	This study	EDE1.F2
CTAAGCACTATCCAACAAAAAGTTAGTGGC GGCTTCTAGAGAATTCGAGCTCGTTTAAAC	This study	EDE1.R1
AATGGCTCAAATAACCGGGGATATACTCT AATTGATTTACGGATCCCCGGGTTAATTAA	This study	ENT1.F2
CATCTGATTAGAAATGCGGACTGGAATGA CAGAATCACTGAATTCGAGCTCGTTTAAAC	This study	ENT1.R1
GGGATATACTCCTGACCAAGGTGTAAGCT TAATTGATCTTCGGATCCCCGGGTTAATTAA	This study	ENT2.F2
TCAAAGATCAATTAAGCTTACACCTTGGTC AGGAGTATATGAATTCGAGCTCGTTTAAAC	This study	ENT2.R1
TAAGAGACACGAATTGCAAGCATTACAAG CAGAAATCAATCGGATCCCCGGGTTAATTAA	This study	END3.F2
AAATATTACACATTCATGTACATAAAATTA ATTATCGGTGGAATTCGAGCTCGTTTAAAC	This study	END3.R1
CAACATATTCAATGCTACTGCATCAAATCC GTTTGGATTCCGGATCCCCGGGTTAATTAA	This study	SLA1.F2
GTTTTAGTTATTATCCTATAAAATCTTAAAATA CATTAAGAATTCGAGCTCGTTTAAAC	This study	SLA1.R1
Recombinant DNA		
pFA6a-GFP(S65T)-His3MX6	Longtine et al.[56]	
pFA6a-GFP(S65T)-kanMX6	Longtine et al.[56]	
pFA6a-3HA-His3MX6	Longtine et al.[56]	
pFA6a-3HA-TRP1	Longtine et al.[56]	
Software and algorithms		
MestReNova Lite CDE	Mestrelab Research	https://mestrelab.com/
Empower™ 3	Waters	https://www.waters.com/
MassLynx™ 4.1	Waters	https://www.waters.com/
GraphPad Prism	GraphPad	https://www.graphpad.com/
Image J	NIH	https://ImageJ.nih.gov/ij/index.html

RESOURCE AVAILABILITY

Lead contact

Further information and requests for resources and reagents should be directed to and will be fulfilled by the Lead Contact, Pau Gorostiza (pau@icrea.cat).

Materials availability

This study did not generate new unique chemical reagents. There are restrictions to the availability of the TL2 peptide due to limited stock. Strains and plasmids generated in this study are available on request to the lead contact.

Data and code availability

- All data reported in this paper will be shared by the lead contact upon request.
- This paper does not report original code.
- Any additional information required to reanalyze the data reported in this paper is available from the lead contact upon request.

EXPERIMENTAL MODEL AND STUDY PARTICIPANT DETAILS

Yeast strains

Yeast strains are listed in the key resources table. Genome-edited strains for fluorescence microscopy and immunoprecipitation assays were constructed by genomic recombination. GFP and HA epitopes were fused at the C-terminus of each protein by homologous recombination in the genome.[57] PCR fragments flanked by 40 base pairs immediately upstream or downstream of the stop codon of the gene of interest were generated using the plasmids pFA6a-GFP(S65T)-*KANMX6*, pFA6a-GFP(S65T)-*HIS3MX6*, pFA6a-3HA-*TRP1* and pFA6a-3HA-*HIS3MX6* plasmids.[57] PCRs were performed with a Vent polymerase (New England Biolabs) and a TRIO-Thermoblock (Biometra GmbH). All plasmids used in this study bear Ampicillin resistance for selection in *E. coli*. Oligonucleotides used in this study are listed in the key resources table. SCMIG1618 was constructed by crossing a lawn of SCMIG1610 with a few cells of SCMIG1214, selecting on SDC-Lys and selecting diploid colonies by microscopic inspection. A few colonies were re-checked for expression of Ent1-HA, Ent2-HA, and Apl3-GFP by immunoblot.

METHOD DETAILS

Synthesis of the photoswitchable crosslinker (BSBCA)

The photoswitchable crosslinker was synthesized adapting a protocol published by Burns et al.[58] All reagents and solvents were purchased from commercial suppliers and were used without any further purification.

NMR spectroscopy

Samples for nuclear magnetic resonance (NMR) were dissolved in either DMSO-d_6 or Water-d_2 (D$_2$O). Spectra were recorded with a Varian Mercury 400 MHz instrument (400 MHz for ^{1}H-NMR) and referenced to residual solvent peaks (DMSO-d_6: ^{1}H 2.50 ppm; D$_2$O: ^{1}H 4.79 ppm). Chemical shifts (δ) are expressed as parts-per-million (ppm) and for azobenzene they refer to the *trans* isomer. Coupling constants (J) are measured in hertz (Hz). Spectra were analysed using MestReNova Lite CDE (Mestrelab Research S.L., Santiago de Compostela, ES).

Synthesis of 2-acetylamino-5-aminobenzenesulfonic acid

A suspension of 2,5-diaminobenzenesulfonic acid (6.47 g, 34.4 mmol) in glacial acetic acid (50 ml) was heated to 94°C under an argon atmosphere. Acetic anhydride (4.0 ml, 42.4 mmol, 1.2 equiv.) was added dropwise to the reaction before refluxing it for 2 h under vigorous stirring. The mixture was hot filtered through a porcelain Büchner funnel and the product repeatedly washed with small quantities of boiling glacial acetic acid (50 ml in total). Upon cooling, the solid was washed with Et$_2$O (2 x 10 ml), dried under reduced pressure and finely grinded. The resulting violet powder was resuspended in refluxing EtOH (50 ml), hot filtered through a Büchner funnel and washed with hot EtOH (2 x 10 ml). The product was dried under high vacuum to give 2-acetylamino-5-aminobenzenesulfonic acid as a light violet solid (6.27 g, 72% yield, 91% purity by ^{1}H NMR). Spectra conformed to those previously described in the literature.[58]

^{1}H NMR (400 MHz, DMSO-d_6): δ 10.36 (s, 1H), 8.39 (d, J = 8.8 Hz, 1H), 7.71 (d, J = 2.7 Hz, 1H), 7.30 (dd, J = 8.6, 2.5 Hz, 1H), 2.08 (s, 3H)

Synthesis of sodium 3,3′-bis(sulfonato)-4,4′-bis-(acetamido)azobenzene

2-acetylamino-5-aminobenzenesulfonic acid (4.00 g, 17.4 mmol) was dissolved in mQ H$_2$O (27 ml) and the pH of the solution was carefully adjusted to 8.5 by small additions of solid Na$_2$CO$_3$. The reaction was immersed in an ice-NaCl mixture and cooled to -5°C before slowly adding a sodium hypochlorite solution (45.6 mL, $\geq$ 13% active chlorine) over 15 min. The flask was covered with aluminium foil to avoid direct contact with light and the mixture was left to stir at -5°C for 2 h and then stored at 4°C for 4 days. The precipitate was filtered through a P5 sintered funnel and washed with hot absolute EtOH (2 x 10 ml). The collected solid was dried under high vacuum to give sodium 3,3′-bis(sulfonato)-4,4′-bis-(acetamido)azobenzene as a yellow powder (405 mg, 9% yield). Spectra matched those previously reported in the literature.[59]

^{1}H NMR (400 MHz, Water-d_2): δ 8.37 (d, J = 2.2 Hz, 2H), 8.15 (d, J = 8.4 Hz, 2H), 8.04 (dd, J = 8.4, 2.2 Hz, 2H), 2.29 (s, 6H)

Synthesis of sodium 3,3′-bis(sulfonato)-4,4′-bis-(amino)azobenzene

To a stirred solution of sodium 3,3′-bis(sulfonato)-4,4′-bis-(acetamido)azobenzene (767 mg, 1.53 mmol) in mQ H_2O (25.6 ml) was added conc. HCl (5.1 ml, 62.1 mmol, 40.5 equiv.). The deep red mixture was refluxed for 2.5 h before letting it cool down to rt. The aqueous solvent was evaporated *in vacuo*, the solid dissolved in mQ H_2O (50 ml) and the pH of the resulting solution adjusted to 8.5 by addition of aqueous NaOH. The product was lyophilized yielding 3,3′-bis(sulfonato)-4,4′-bis-(amino)azobenzene as an orange solid (600 mg, 94% yield). Spectra conformed to those previously described in the literature.[59]

^{1}H NMR (400 MHz, DMSO-d_6): δ 7.94 (d, J = 2.4 Hz, 2H), 7.52 (dd, J = 8.7, 2.4 Hz, 2H), 6.70 (d, J = 8.6 Hz, 2H), 6.19 (s, 4H)

Synthesis of BSBCA

In a 50 mL reaction flask sodium 3,3′-bis(sulfonato)-4,4′-bis-(amino)azobenzene (429 mg, 1.03 mmol) was mixed with chloroacetic acid (2.92 g, 30.9 mmol, 30.0 equiv.) and chloroacetic anhydride (5.29 g, 30.9 mmol, 30.0 equiv.). This solid mixture was heated above its reactants melting point and left to stir at 87°C overnight. BSBCA was precipitated upon cooling the reaction over ice for at least 30 min. The resulting solid was filtered off via a P4 sintered funnel, washed with dichloromethane (5 x 20 ml) and dried on the high vacuum line. This afforded the desired compound as a yellow solid (450 mg, 77% yield). Spectra matched those previously reported in the literature.[59]

^{1}H NMR (400 MHz, DMSO-d_6) δ 11.22 (s, 2H), 8.53 (d, J = 8.8 Hz, 2H), 8.20 (d, J = 2.4 Hz, 2H), 7.98 (dd, J = 8.8, 2.4 Hz, 2H), 4.42 (s, 4H).

TL2 crosslinking procedure

Uncrosslinked TL2 (purity >85%) was purchased from a custom peptide synthesis service (Ontores Biotechnologies Inc., Hangzhou, CN) and stapled with the BSBCA crosslinker following the procedure described by Nevola et al.[25] Uncrosslinked TL2 (5 mg) was dissolved in 1.5 ml of freshly prepared 50 mM Tris-HCl buffer (pH 8.3–8.4) supplemented with 10 mM tris-(2-carboxyethyl)phosphine (TCEP). The peptide Cys residues were allowed to reduce at rt for 1 h in a closed vial. BSBCA (3.35 mg, 6.40 μmol, 3 equiv.) was dissolved in 300 μl of reaction buffer and added to the peptide solution over 3 hours (1 equiv. per hour). The mixture was kept protected from light and stirred overnight at rt. The reaction was followed by UPLC and the formation of the desired product was verified by UPLC-MS. Upon completion, the crude mixture was lyophilized and purified by HPLC.

Peptide isolation

The crude peptide was dissolved in mQ H_2O and purified by HPLC. The system consisted of a Waters Alliance e2695 Separations Module equipped with an automatic injector and a Waters 2998 UV/Vis Photodiode Array Detector (Waters, Milford, MA). Samples (between 20 and 100 μl) were injected on a SunFire® C18 column (100 Å, 5 μm, 150 x 4.6 mm). The mobile phase was a mixture of mQ H_2O and acetonitrile respectively supplemented with 0.045% and 0.036% trifluoroacetic acid - TFA (v/v). Purification was carried out at rt applying a 20 to 35% 8-min linear gradient while keeping the flow rate at 1 ml/min. Data were acquired using the Empower™ 3 software. To allow manual collection of the fractions, the waste tube coming out from the detector was replaced with a short rigid outlet. The eluate was collected at the appropriate retention time, while monitoring the run at both 220 and 365 nm. The corresponding fractions were then pooled together, analysed by UPLC and UPLC-MS, and lyophilized.

TL2 analytical characterization

UPLC and UPLC-MS analysis were performed with an ACQUITY UPLC H-Class System (Waters, Milford, MA) equipped with a Flow Through Needle-Sample Manager (SM-FTN), column heater, quaternary solvent manager and an ACQUITY UPLC Photodiode Array (PDA) eλ Detector. UPLC-MS mass spectra were obtained with a SQ Detector2 (Waters) equipped with an electrospray ionization (ESI) interface. Empower™ 3 and MassLynx™ 4.1 were respectively used as software for data acquisition. The analysis was run on an ACQUITY BEH C18 (130 Å, 1.7 μm, 50 x 2 mm) column, which was maintained at 40°C. The mobile phase was a mixture of mQ H_2O and acetonitrile respectively supplemented with either 0.045% and 0.036% TFA (v/v) for UPLC analysis or 0.1% and 0.07% formic acid - FA (v/v) for UPLC-MS. The flow rate was maintained at 0.6 ml/min while applying 25 to 35% 2-min long linear gradients. Samples were analysed as eluted or as lyophilized solid redissolved in mQ H_2O and filtered through a 0.22 μm filter. Detection was performed at 220 and 365 nm.

UPLC purity: 98%

UPLC-MS (ESI): *m/z* calculated for $C_{115}H_{168}N_{32}O_{42}S_5^{2+}$ [M+2H]$^{2+}$: 1414.52; found: 1414.94.

Peptide quantification

Lyophilized samples were reconstituted in 50 mM phosphate-buffered saline (PBS, pH 7.4) at 10x their final concentration and quantified by measuring the absorption of the azobenzene moiety at 363 nm (ε_{363} = 24000 $M^{-1}cm^{-1}$) with a micro-volume spectrophotometer (NanoDrop™ 2000 Spectrophotometer, ThermoScientific).

Yeast growth conditions

All strains were maintained on Petri plates containing the appropriate growth medium supplemented with 2% agar. Rich YPD medium (1% yeast extract, 2% peptone and 2% glucose) was used to culture strains of *Saccharomyces cerevisiae*. *Schizosaccharomyces pombe* cells were grown in YE5S medium (0.5% Difco yeast extract, 3% glucose, 0.025% His, 0.025% Leu and 0.025% Ura). The composition of the SDC-Trp medium was as follows: 0.67% yeast nitrogen base, 2% glucose, 0.075% complete supplement mixture (CSM)-Trp. In all the experiments, cells were grown at 25°C under vigorous shaking in Erlenmeyer flasks containing 50 ml of the corresponding growth media. In the morning of the assay, the culture was diluted to an OD_{600} of 0.2 and grown till early log phase (0.45-0.55 OD_{600}) before being harvested.

Peptide uptake in yeast

From an early log-phase culture, 1.5 ml of cell suspension was harvested and centrifuged for 5 min at 5100 g. The supernatant was replaced with 20 µl of SDC-Trp medium (YE5S medium for *S. pombe*) containing Protease Inhibitors (PIs) and 100 µM TL2, either fluorescently labelled or not. Cells were incubated at 30°C with gentle shaking and for increasing time intervals (1 hour maximum) before being washed twice and resuspended in 10 µl of medium. Equal volumes of the resulting cell suspension and 1.6% melted agarose (Low Melt Agarose, Bio-Rad, Barcelona, ES) were then mixed and an aliquot was placed on a microscope slide for imaging. In both mock- and TL2-treated samples, PIs were used at the following final concentrations from a freshly prepared 10x mix: 0.5 mM PMSF, 5 µg/ml Leupeptin, 2,5 µg/ml Antipain, 1 µg/ml Pepstatin and 1 µg/ml Aprotinin.

S. Cerevisiae spheroplasts preparation

Lyticase from Arthrobacter luteus (≥2,000 units/mg protein; protein ≥20 % by biuret) was purchased from Sigma-Aldrich (Munich, DE) and reconstituted in mQ water. Cells were grown in early exponential phase to harvest 15 ml of culture. The suspension was centrifuged for 3 min at 4700 g, washed and the pellet resuspended in half the original volume with 0.1 M Tris HCl (pH 9) supplemented with 10 mM 2-mercaptoethanol. After 10 min incubation at rt and 100 rpm orbital shaking, the culture was washed with 10 ml of spheroplasting buffer (10 mM Tris HCl pH 7.0, 0.7 M sorbitol, 5% glucose, 0.5x YPD-Trp). Cells were collected by centrifugation, resuspended in 1 ml of spheroplasting buffer, and incubated at 30°C and 350 rpm in the presence of 100 u/ml lyticase. After 30 min, the suspension was centrifuged (3 min at 700 g), washed with SDC-Trp supplemented with 0.7 M sorbitol and resuspended in 0.4 ml of the same medium (17-21 OD_{600} U/ml).

Peptide uptake in spheroplasts

Spheroplasts were aliquoted (100 µl per condition, 17-21 OD_{600} U/ml) in Eppendorf tubes and centrifuged for 3 min at 700 g. The supernatant was replaced with 20 µl of uptake buffer (SDC-Trp medium supplemented with 0.7 M sorbitol, 30 µM TL2 – either fluorescently labelled or not – and PIs). After 10 min of pre-incubation at room temperature and 350 rpm, FM4-64 (16 µM final concentration) was added to the suspension and the incubation continued for further 5 min. Spheroplasts were then washed with SDC-Trp medium containing 0.7 M sorbitol, spun down and incubated with 20 µl of fresh uptake buffer for further 40 min. For imaging, cells were washed twice and mounted with low-melting point agarose as previously described. The endocytic marker FM4-64 (Molecular Probes, Eugene, USA) was prepared as a 16 mM stock solution in DMSO. In both mock- and TL2-treated samples, PIs were used at the following final concentrations from a freshly prepared 10x mix: 0.5 mM PMSF, 5 µg/ml Leupeptin, 2,5 µg/ml Antipain, 1 µg/ml Pepstatin and 1 µg/ml Aprotinin.

Cortical patch dynamics

Spheroplasts were aliquoted (100 µl per condition, 17-21 OD_{600} U/ml) in Eppendorf tubes and centrifuged for 3 min at 700 g. The supernatant was replaced with 20 µl of SDC-Trp medium supplemented with 0.7 M sorbitol, 100 µM TL2 (pre-illuminated either at 380 or 500 nm), and PIs. Cells were incubated in the dark at 30°C and 350 rpm and analysed at different time points (10, 20 and 30 min) as wet mounts in SDC-Trp medium supplemented with 0.7 M sorbitol. In both mock- and TL2-treated samples, PIs were used at the following final concentrations from a freshly prepared 10x mix: 0.5 mM PMSF, 5 µg/ml Leupeptin, 2,5 µg/ml Antipain, 1 µg/ml Pepstatin and 1 µg/ml Aprotinin. Medium containing TL2 or vehicle was irradiated for at least 10 min with a custom-made multi-LED dual wavelength (380/500 nm) lamp (FC Tecnics, Barcelona, ES) before being added to the cells. To prevent thermal relaxation of pre-activated TL2, vehicle- and peptide-treated samples were exposed to 30 s of UV light after 15 min of incubation.

For *in situ* TL2 activation experiments (Figures 3D and 3E), spheroplasts were treated with 20 µl of SDC-Trp medium supplemented with 0.7 M sorbitol, 100 µM dark-adapted TL2 and the above-described PI cocktail. Cells were incubated in the dark at 30°C and 350 rpm and analysed at different time points (25 min for TL2-treated spheroplasts and 30 min for mock-treated samples) as wet mounts in SDC-Trp medium supplemented with 0.7 M sorbitol. Movies were then acquired at 2 s intervals for 2 min before and after irradiation. To irradiate the sample, the microscope condenser was carefully lifted and the slide was illuminated from the top with 380 nm UV light for 1 minute.

Fluorescence microscopy

Fluorescence microscopy was performed as described by Del Dedo et al.[21] Samples were viewed on a Leica DMI6000 wide-field microscope equipped with a 63x APO (NA=1.4) oil immersion objective. Images were acquired at rt using a Hamamatsu Orca-R2 camera controlled by the Leica Application Suite X (LAS_X) software. Fluorescence was visualized with appropriate filter sets mounted on an ultrafast external wheel

and illuminated by a SOLA-SMII white LED light. GFP or carboxyfluorescein and FM4-64 were excited through BP470/40 and BP572/35 filters, respectively. Emitted light was detected with BP521/40 (green) and BP632/62 (red) filters. Movies were acquired at 2 s intervals for 2 min.

Samples from Figures 2B and 4 were imaged on a Leica Thunder 3D live cell, equipped with a 63× water immersion lens (NA 1.2), a fast and sensitive sCMOS camera DFC9000 and a Spectra-X Light Engine. The GFP was excited using a BP475/28 filter and the emitted light was detected with a BP510/40 filter. As described above, movies were acquired at 2 s intervals for 2 min.

Immunoprecipitation and immunoblots

For the anti-GFP-agarose immunoprecipitations, cells were glass bead-lysed in LB (25 mM Tris, 5 mM EDTA, pH 8.5) in the presence of protease inhibitors (PIs) (1 mM PMSF, 5 μg/ml Leupeptin, 2.5 μg/ml Antipain, 1 μg/ml Pepstatin and 1 μg/ml Aprotinin). Unbroken cells were eliminated at 700 g for 15 minutes at 4°C. The supernatant was diluted with the same volume of BB (10 mM Tris, 0.2 mM EDTA, 0.2 mM DTT, pH 7.5) containing PIs. The post 700 g supernatants were spun at 13,000 g for 20 minutes, the pellet was recovered and resuspended in 1 ml of IP buffer (50 mM Tris, 150 mM NaCl, 5 mM EDTA, 1% Triton X-100, pH 7.5). The extract was adjusted to 1 mg of protein/ml, incubated 30 minutes at 4°C and spun at 700 g for 15 minutes. The supernatant was incubated with 20 μl of 50% anti-GFP-Agarose (GFP-trap, Chromotek) for 1 h at 4°C. Beads were washed with IP, and subsequently with IP buffer without Triton X-100 and boiled in 25 μl SDS-PAGE sample buffer. SDS–PAGE was performed as described[59] using pre-casted Mini-PROTEAN TGX 4-20% Acrylamide gels (Bio-Rad). For immunoblot, nitrocellulose membranes (Protan BA85, GE Healthcare) were probed with anti-HA (Anti-HA-Peroxidase High Affinity 3F10, Roche) or anti-GFP (Monoclonal Antibody (JL-8), Living Colors), followed by a peroxidase-conjugated secondary goat anti-rabbit IgG antibody (Sigma Aldrich). Protein transfer, blotting and chemiluminescence detection were performed using standard procedures. Detection of proteins was performed using the ECL kit (GE Healthcare).

QUANTIFICATION AND STATISTICAL ANALYSIS

ImageJ[60] (NIH, Bethesda, USA) was used to adjust image size, brightness, and contrast in Figure 2, and to project and quantify Sla1-GFP kymographs for Figures 3, 4, and S1. In Figure 3I and S1E, fluorescence intensity was plotted after subtracting the relative background intensity with Microsoft Excel. All graphs were created with GraphPad Prism v8.3.1 (GraphPad Software, San Diego, USA). Statistical analysis was performed either with GraphPad Prism or Microsoft Excel. Unless otherwise stated, statistical differences were determined by Student's t test (n.s., not significant; *, p-value<0.05; ***, p-value<0.01; ****, p-value<0.001). Details on the experimental n and on the number of replicates are included for each experiment in the corresponding figure legend.